frontiers | Frontiers in Astronomy and Space Sciences

TYPE Original Research
PUBLISHED 05 August 2024
DOI 10.3389/fspas.2024.1427791

OPEN ACCESS

EDITED BY
Yu Lin,
Auburn University, United States

REVIEWED BY
Binbin Tang,
Chinese Academy of Sciences (CAS), China
Xuanye Ma,
Embry–Riddle Aeronautical University, United States

*CORRESPONDENCE
B. Michotte de Welle,
bayane.michotte-de-welle@lpp.polytechnique.fr

RECEIVED 04 May 2024
ACCEPTED 04 July 2024
PUBLISHED 05 August 2024

CITATION
Michotte de Welle B, Aunai N, Lavraud B, Génot V, Jeandet A, Nguyen G, Ghisalberti A and Smets R (2024), Spatial distribution of plasma density and magnetic field amplitude in the dayside magnetosheath as a function of the IMF orientation.
Front. Astron. Space Sci. 11:1427791.
doi: 10.3389/fspas.2024.1427791

Spatial distribution of plasma density and magnetic field amplitude in the dayside magnetosheath as a function of the IMF orientation

B. Michotte de Welle[1]*, N. Aunai[1], B. Lavraud[2], V. Génot[3], A. Jeandet[1], G. Nguyen[4], A. Ghisalberti[1] and R. Smets[1]

[1]CNRS, Ecole Polytechnique, Sorbonne Université, Université Paris Sud, Observatoire de Paris, Institut Polytechnique de Paris, Université Paris-Saclay, PSL Research Univsersity, Laboratoire de Physique des Plasmas, Palaiseau, France, [2]Laboratoire d'Astrophysique de Bordeaux, Université Bordeaux, CNRS, Pessac, France, [3]Institut de Recherche en Astrophysique et Planétologie, CNRS, Université de Toulouse, CNES, Toulouse, France, [4]DPHY, ONERA, Université de Toulouse, Toulouse, France

The properties of the magnetosheath are of pivotal importance in determining the coupling between the magnetosphere and interplanetary medium. In particular, the magnetic flux pileup and plasma depletion layer (PDL) modify the boundary conditions of magnetopause reconnection. However, the spatial distribution of the magnetic field strength and plasma density in the magnetosheath and their functional dependence on the interplanetary magnetic field (IMF) orientation remain poorly understood. This study characterizes these aspects in detail through the statistical processing of decades of data from Cluster, Double Star, THEMIS, and Magnetospheric Multiscale (MMS) missions. The first part of this study focuses on the poorly known variations across the magnetosheath, from the shock to the magnetopause. The magnetic pileup and PDL are significantly correlated, with a strong dependence on the IMF cone angle. Their dependence on the IMF clock angle is found only near the magnetopause, consistent with the expected effect of magnetic reconnection. The second part of this study examines the asymmetry in the magnetic field amplitude and density between the quasi-parallel and quasi-perpendicular sides of the equatorial magnetosheath. These asymmetries are characterized for different relative distances to the magnetopause and bow shock boundaries and for different IMF orientation. The magnetic field amplitude, observed to be higher on the quasi-perpendicular side of the magnetosheath, becomes more symmetric as it approaches the magnetopause. The quasi-parallel magnetosheath exhibits a higher plasma density near the magnetopause. However, this asymmetry reverses at approximately the mid-magnetosheath with a decreasing IMF cone angle.

KEYWORDS

magnetosheath, magnetic pileup, plasma depletion layer, asymmetry, plasma density, magnetic field amplitude, magnetopause

1 Introduction

Upon reaching the Earth's magnetosphere obstacle, the solar wind decelerates to a subsonic speed, compresses, and experiences a significant increase in the amplitude of the interplanetary magnetic field (IMF) in a region called the magnetosheath. The fundamental properties of the magnetosheath, in particular the way the plasma and magnetic field are spatially distributed and structured in that region, greatly determine the subsequent evolution of the magnetosphere as they represent the immediate boundary condition for all processes occurring at the magnetopause. This includes magnetic reconnection, the process known to open the magnetosphere to incoming solar wind and interplanetary magnetic flux. The main parameter governing how reconnection proceeds at the magnetopause is probably the orientation of the IMF and, more concretely, the specific way the IMF drapes around the magnetopause and establishes a more or less pronounced magnetic shear across the boundary. The draping of the magnetic field and the subsequent magnetic shear at the magnetopause have thus been studied and used in many works to constrain magnetic reconnection therein (Kobel and Fluckiger, 1994; Cooling et al., 2001; Romashets and Vandas, 2019; Trattner et al., 2021; Michotte de Welle et al., 2022). However, magnetic reconnection will also be greatly impacted by the magnetic field amplitude and plasma density distribution adjacent to the magnetopause since these quantities primarily control the rate at which the IMF is reconnected to the geomagnetic field (Cassak and Shay, 2007). Much less is known, however, about the spatial variation of field amplitude and plasma density throughout the magnetosheath and up to the close proximity of the magnetopause. Investigating spatial profiles in the magnetosheath and their dependence on upstream interplanetary conditions is challenging from an observational standpoint due to the local character of *in situ* measurements, the entanglement of the inherent temporal and spatial variations, and the scarcity of data.

On a large scale and as a first approximation, the interplanetary magnetic flux and plasma cannot penetrate the magnetopause. The plasma and magnetic flux thus have no other way than to pile up on the obstacle and flow around it. The reality is, however, a bit more complex than this simple picture, which was originally obtained from gas dynamics models (Spreiter et al., 1966).

The first complexity arises from the interplay between the plasma and magnetic field, which do not independently pile up onto the magnetopause from one another. As the magnetic amplitude increases, the plasma is increasingly squeezed out and its density progressively drops near the magnetopause. This so-called depletion layer, theorized as a pure magnetohydrodynamics (MHD) effect (Zwan and Wolf, 1976), has been reported in various observations (Paschmann et al., 1978; Crooker et al., 1979; Hall et al., 1990; Sibeck et al., 1990; Song et al., 1990; Fuselier et al., 1991; Paschmann et al., 1993; Phan et al., 1994; Anderson et al., 1997; Pudovkin et al., 2001; Šafránková et al., 2002). This effect has also been observed and investigated in global MHD simulations (Wu, 1992; Wang et al., 2003; Wang et al., 2004a; Wang et al., 2004b; Borovsky et al., 2008), which have shown a high dependence on the solar wind Mach number. This is well understood since the Mach number essentially determines the plasma β within the magnetosheath and, therefore, the extent to which the enhanced magnetic field amplitude can lead to plasma depletion. The magnetic pileup and associated plasma depletion layers have since been observed and studied upstream of other planets (Øieroset et al., 2004; Gershman et al., 2013; Masters et al., 2014) or at the heliopause (Cairns and Fuselier, 2017).

The second complexity comes from the fact that the magnetic flux pileup and the associated plasma depletion layer are not only the coupled consequences of the large-scale impact of the magnetized solar wind with the impenetrable magnetospheric obstacle. In reality, magnetopause reconnection enables part of the magnetic and plasma fluxes to penetrate within the magnetosphere rather than flowing around it in the magnetosheath. Therefore, characterizing these features of the magnetosheath becomes even more complex when realizing that in nonlinear feedback, reconnection itself will impact how pronounced and deep the flux pileup and depletion layer, respectively, are (Anderson et al., 1997). Investigating the dependence of the magnetic flux pileup and plasma depletion layer properties on the upstream IMF orientation is important not only for better constraining magnetopause reconnection but also for understanding the extent to which reconnection influences these magnetosheath properties.

Several studies have thus specifically focused on the functional dependence of the flux pileup and plasma depletion layer (PDL) on the IMF orientation. In the absence of a solar wind monitoring spacecraft, this has often been done indirectly by correlating the PDL and pileup properties to the local magnetic shear at the magnetopause. These observations have revealed many interesting aspects of the pileup and PDL. Using straight crossings of the magnetopause from ISEE, Paschmann et al. (1978) identified PDL signatures in the data and estimated that the region had a thickness of approximately 0.1–0.3 R_e. Using 22 AMPTE/IRM low-latitude magnetopause crossings in low magnetic shear (<30°) conditions, Paschmann et al. (1993) later reported that only half of the events revealed signatures of pileup and plasma depletion, for which the thickness would be of the order of 0.3–0.4R_e. In another case study, Šafránková et al. (2002) reported thicknesses of the order of 0.6–1 R_e. Anderson and Fuselier (1993) reported weaker PDL signatures for negative B_z than for northward conditions, suggesting the underlying role of reconnection in regulating the PDL and pileup properties. Soon after, Phan et al. (1994) analyzed 38 AMPTE/IRM magnetopause crossings spanning most of the low-latitude dayside region. The authors distinguish low shear (<30°) from high shear (>60°) crossings and found, from a superposed epoch analysis, that, on average, a PDL associated with a magnetic flux pileup only exists in the former case. For shears greater than 60°, neither magnetic pileup nor PDL is observed, leading to the conclusion that reconnection at the magnetopause, which would operate under these shear conditions, is transferring magnetic flux across the boundary instead of forcing it to pile up against it. The role of magnetopause reconnection in shaping the specific properties of the pileup and PDL was later more strongly emphasized by Anderson et al. (1997). They revealed that PDL signatures weaken as the magnetic shear increases, but they can still be observed under high shears in large β conditions, suggesting that the reconnection rate may not be able to match the driving imposed by the solar wind electric field. The rather general occurrence of a gradual density decrease approaching the magnetopause independently from the

sign of the local IMF B_z had later been confirmed in case studies by Pudovkin et al. (2001); Šafránková et al. (2002).

By the early 2000s, research on the properties of the magnetic pileup and associated PDL started to lose momentum. The complexity of the system, unsteady upstream interplanetary conditions, magnetosheath turbulence, and scarcity of *in situ* single spacecraft measurements somehow hampered further progress. The precise characterization of the depth and thickness of the PDL and the intensity of the magnetic pileup, their precise functional dependence on the IMF orientation, and their spatial structure beyond the subsolar region were extremely difficult to investigate observationally. More global and parametric studies of the magnetic pileup and PDL properties became accessible only via well-resolved global MHD modeling (Wang et al., 2003; Wang et al., 2004a; Dorelli et al., 2004). Simulations revealed that isotropic MHD is enough to capture the essence of the PDL properties, and pressure anisotropies often observed in the PDL (Paschmann et al., 1993) are a consequence rather than a cause of the existence of the layer. They revealed that the PDL extends away from the subsolar region in magnetic local time and latitude although the magnetic and density profiles become increasingly shallower. Wang et al. (2004b) revealed a negligible dependence of the PDL structure on different IMF clock angles, varying from 0° to 45°. A parametric study for larger clock angles, which would allow a precise investigation of the role of reconnection, has never been performed. It is expected that radial IMF leads to weak or no global magnetic pileup and, thus, no PDL either. However, as for the clock angle, although accessible to modern numerical models, a parametric study on the pileup and PDL properties for varying IMF cone angles from 0° to 90° has never been performed.

Over the years, vast amounts of data have been accumulated from multiple missions spanning decades of explorations of the Earth's magnetosphere and nearby interplanetary space. The compilation of large datasets has subsequently enabled us to revisit the problem of the spatial variations of fundamental plasma and field properties in the system. Several studies have, over the last decade, revisited the characterization of magnetosheath properties from a global and statistical perspective (Dimmock and Nykyri, 2013; Dimmock et al., 2014; 2016; 2020; Zhang et al., 2019; Ma et al., 2020; Michotte de Welle et al., 2022). Using a large dataset combining THEMIS and Cluster measurements, Zhang et al. (2019) showed that the profile of the magnetic amplitude reconstructed along the Sun–Earth line increases rather monotonously across the subsolar magnetosheath. They revealed that this profile depends on the IMF cone angle, with lower amplitudes for more radial IMFs, as expected. However, no dependence of the profile on the IMF clock angle was found. The magnetic profiles obtained in the study exhibit a sharp increase from the middle of the magnetosheath upon approaching the magnetopause. The authors suggested that these divergent profiles are the result of incorrect placement of magnetosphere measurements on the magnetosheath side of the magnetopause due to inaccuracies in the analytical boundary models that were used. The density profiles obtained throughout the subsolar magnetosheath typically exhibit a bell curve shape, from the bow shock to the magnetopause, independent of any interplanetary conditions, including the IMF orientation. The density shows a gradual decrease toward the magnetopause from the middle of the magnetosheath. However, being collocated with the aforementioned ramp of the magnetic field and independent of the IMF orientation, this gradual decrease is more likely the coarse-grained representation of the density transition across the magnetopause than the actual signature of the PDL. Resolving the PDL scale and, more generally, spatial variations across the magnetosheath thickness appears very challenging, particularly in the subsolar region, where the magnetosheath is typically thick of only few Earth radii. Improving ways to extract and reposition magnetosheath measurements appears as critical as using several measurements to lower statistical noise.

Studies using statistical spatial reconstructions have thus rather focused on the longitudinal variations and, more specifically, on characterizing and understanding the cause of the asymmetries observed between the dawn and dusk sides of the magnetosheath, particularly in the plasma density. Observations generally report a larger particle density on the dawn side than on the dusk side. Considering the average Parker spiral structure of the IMF, the dawn side typically tends to be the quasi-parallel side of the bow shock, making the IMF orientation a natural candidate for the source of the observed asymmetry. Using isotropic Rankine–Hugoniot MHD jump conditions and a modeled shock boundary, Walters (1964) theorized the existence of an asymmetry with somewhat larger densities on the quasi-parallel dayside magnetosheath just downstream of the bow shock. A clear correlation between the existence and level of the asymmetry and the IMF orientation has, however, not yet been firmly established. Paularena et al. (2001) reported 30% larger densities in the dawn nightside magnetosheath ($-20R_e < X_{GSE} < -15R_e$) that seem to disappear during the quiet part of the solar cycle, but without clear correlation with the orientation of the IMF. Němeček et al. (2002) reported a 20% larger ion flux on the dawn side in a somewhat more earthward region ($-15R_e < X_{GSE} < 5R_e$) without firmly establishing the causal link to the IMF orientation either. Longmore et al. (2005), using the Cluster measurements, found lower densities measured on the dawn side of the magnetosheath in the northern hemisphere and also did not find a correlation between the IMF orientation and the observed asymmetry. Using THEMIS data, Walsh et al. (2012) reported a 20% larger dawn density, but this time, it was only near the dayside magnetopause. Although, on average, the dawn region is more likely to represent the quasi-parallel side of the magnetosheath, large IMF variations often lead to the exact inverse situation, particularly during active periods of the solar cycle. Averaging measurements made in the dawn sector, regardless of the upstream IMF orientation obtained via a solar wind monitor, likely mixes quasi-parallel and quasi-perpendicular magnetosheath data. This samples a very different magnetic environment, thereby precluding the possibility of establishing a firm IMF causality. To address this issue, Dimmock and Nykyri (2013) transformed the data in the MPIM coordinate system, where each measurement is rotated into the "right" sector of the magnetosheath according to the upstream IMF, but no clear asymmetry was observed. Using a similar procedure, but this time focusing on the nearby magnetopause magnetosheath, Dimmock et al. (2016) then found a density asymmetry increasing from noon to the terminator.

Recently, Michotte de Welle et al. (2022) used a vast amount of data from multiple missions to reconstruct the structure of the magnetic field draping around the magnetopause. In this study, the key steps of magnetosheath data extraction and repositioning

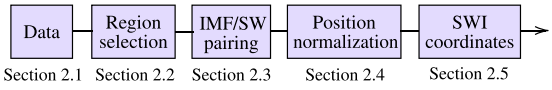

FIGURE 1
Overview of the pre-processing pipeline of Michotte de Welle et al. (2022) for preparing the dataset used in this study.

were significantly improved through the use of machine learning models. This enabled a detailed 3D and global reconstruction of the draping structure with unprecedented resolution, both spatially and in dependence on the upstream IMF orientation. The same technique was subsequently used to extract the plasma density along with the previously obtained magnetic field and reconstruct global maps of the magnetic shear, current density, and reconnection rate scaling law on the dayside magnetopause for any IMF clock and cone angle (Michotte de Welle et al., 2024). In this paper, we propose to use the same large magnetosheath dataset to revisit the problem of characterizing the magnetic flux pileup, plasma depletion layer, and density asymmetry in the dayside magnetosheath as a function of the IMF orientation. Section 2 provides a review of the key steps involved in the preparation of the dataset used in this study and performed by Michotte de Welle et al. (2022); Michotte de Welle et al. (2024) and explains the new technical aspects introduced in the current work. Section 3 presents the results obtained about the characterization of the magnetic flux pileup and PDL, while Section 4 focuses on those regarding the density asymmetry throughout the magnetosheath. Section 5 provides the discussion and conclusion of this study.

2 Methods

This study uses a multi-mission dataset of magnetosheath measurements, already used by Michotte de Welle et al. (2022); Michotte de Welle et al. (2024). Measurements have been pre-processed in these studies so that each data point is paired with upstream interplanetary conditions and repositioned in between a single pair of magnetopause and bow shock boundaries. The work described in this article starts with this ensemble of pre-processed magnetosheath data points. For the sake of clarity, this section briefly reviews the key steps of pre-processing, which are represented in Figure 1 and otherwise extensively detailed by Michotte de Welle et al. (2022); Michotte de Welle et al. (2024). Additionally, the spatial distribution of the measurements for each step of the pipeline of this study can be found in Michotte de Welle et al. (2024). Lastly, we detail the techniques specifically employed in this study to investigate spatial profiles across the subsolar magnetosheath and asymmetries between its quasi-parallel and quasi-perpendicular sides.

2.1 Data usage

The dataset compiles measurements obtained by Cluster, Double Star, THEMIS, and Magnetospheric Multiscale (MMS) missions. These missions have consistently provided data for a significant period of time on both equatorial and polar orbits with few limitations, making them ideal for automatic handling. Table 1 provides an overview of the missions, probes, periods, and instruments used in this study. The plasma and magnetic field measurements from all missions are resampled at 5 s resolutions. Additionally, the OMNI data (King and Papitashvili, 2005) are used, specifically including magnetic field, plasma bulk velocity, ion particle density, ion temperature, dynamic pressure, plasma beta, Mach number, and bow shock subsolar point position at 1-min resolution from 2000 to 2021, resampled at the same cadence as the previous data.

2.2 Extraction of the magnetosheath measurements

The first step of data processing consisted of automatically selecting, per spacecraft, time intervals during which measurements were made in the dayside magnetosheath. To minimize erroneous selection of measurements in the magnetosphere or solar wind, a gradient-boosting classifier was used to extract *in situ* plasma data. The classifier, trained in previous studies (Michotte de Welle et al., 2022; Nguyen et al., 2022; Michotte de Welle et al., 2024), provides a point-wise classification of the data into the magnetosphere, solar wind, or magnetosheath regions based on plasma density, bulk velocity, temperature, and magnetic field. This first step ends with 50 million 5-s resolution magnetosheath measurements extracted across all considered spacecraft.

2.3 Pairing measurements with upstream solar wind properties

The second step consisted of pairing each measurement with an upstream solar wind and IMF condition. This is necessary in order to obtain the functional dependence of the magnetosheath properties on the IMF orientation by slicing our dataset for specific ranges of orientations. Another use of this pairing is to obtain the distance of each measurement to the magnetopause and bow shock boundaries from models parametrized by these interplanetary conditions. This relative distance estimate is needed to reposition data points in between a standard system of boundaries, as explained in the following section. Lastly, these paired interplanetary data are used to normalize the magnetosheath measurements. To account for the propagation up to the spacecraft, solar wind properties were selected at a time shifted from the measurement time using a propagation method adapted from Šafránková et al. (2002). An initial propagation time was estimated based on the spacecraft's radial distance to the bow shock, where OMNI data are defined, and an average solar wind speed (400 kms^{-1}). Then, the solar wind velocity was obtained from OMNI data averaged over a 5-min window centered on the estimated propagation time shift. The final values of solar wind and

TABLE 1 Source of the *in situ* data.

Mission	Probe	Period	Instrument
Cluster	C1	2001–2019	Cluster ion spectrometry (CIS) (Rème et al., 2001) Fluxgate magnetometer (FGM) (Balogh et al., 2001)
	C3	2001–2009	
DoubleStar	TC1	2004–2007	Hot ion analyzer (HIA) (Rème et al., 2005 Fluxgate magnetometer (FGM) (Carr et al., 2005)
THEMIS	A, D, E	2007–2021	Electrostatic analyzer (ESA) (McFadden et al., 2008) Fluxgate magnetometer (FGM) (Auster et al., 2008)
	B, C	2007–2009	
Magnetospheric Multiscale	MMS1	2015–2021	Plasma investigation (FPI) (Pollock et al., 2016) Fluxgate magnetometer (FGM) (Russell et al., 2016)
OMNI	N/A	2001–2021	

IMF parameters were obtained by determining a new time shift based on the updated solar wind speed. Data points for which there are no OMNI data have been discarded, lowering the total number of usable magnetosheath measurements to 46 million.

2.4 Repositioning of measurements relative to the magnetopause and bow shock

Two points in the dataset with the same absolute position may be at vastly different distances from the magnetopause and bow shock due to potentially different solar wind and IMF conditions at the time of measurement. In order for studies such as this to avoid mixing measurements made at different relative distances from the boundaries, measurements in the dataset had to be repositioned between a single pair of boundaries to reflect their estimated relative distances accurately. The distance to the magnetopause and bow shock of each point was estimated by Michotte de Welle et al. (2022) using two gradient-boosting regression (GBR) models of the boundaries. These machine learning models predict the radial distance of the bow shock and magnetopause for a given angular direction and interplanetary conditions. They were trained on 30,000 (resp. 20,000) magnetopause (resp. bow shock) crossings. Analytical models have also been used to reposition measurements, as demonstrated by Zhang et al. (2019); Dimmock and Nykyri (2013); Dimmock et al. (2016). However, the significant error made in these models' predictions, in comparison to the machine learning models, results in a larger spurious spatial mixing scale of measurements, thereby lowering the final spatial resolution. Due to the remaining inaccuracies in the boundary models or the prior error in determining the precise causal upstream interplanetary conditions, some measurements are found to be too far outside their predicted boundaries and are, therefore, discarded. After being repositioned, the magnetosheath dataset contains approximately 45 million measurements.

2.5 Solar wind interplanetary magnetic field coordinate system

The final step in making the dataset used in this study consisted of transforming the measurements from the GSM coordinate system to the solar wind interplanetary (SWI) magnetic field coordinate system (Zhang et al., 2019). This coordinate system ensures that each point is located in the appropriate sector of the magnetosheath, either quasi-parallel or quasi-perpendicular, based on its causal IMF. The X_{SWI} axis is anti-parallel to the solar wind velocity vector ($\mathbf{V}_{sw}$), while Y_{SWI} is along the direction of the IMF ($\mathbf{B}_{imf}$) component orthogonal to the X_{SWI} axis, with B_{ximf} always being positive. Eq. 1 provides the unit vectors of the SWI basis for each magnetosheath measurements.

$$\begin{cases} \widehat{\mathbf{X}}_{\mathrm{SWI}} &= -\mathbf{V}_{sw}/\|\mathbf{V}_{sw}\| \\ \widehat{\mathbf{Y}}_{\mathrm{SWI}} &= \widehat{\mathbf{Z}}_{\mathrm{SWI}} \times \widehat{\mathbf{X}}_{\mathrm{SWI}} \\ \widehat{\mathbf{Z}}_{\mathrm{SWI}} &= \left(\widehat{\mathbf{X}}_{\mathrm{SWI}} \times \frac{Bx_{imf}}{|Bx_{imf}|}\mathbf{B}_{imf}\right) \Big/ \left\|\widehat{\mathbf{X}}_{\mathrm{SWI}} \times \frac{Bx_{imf}}{|Bx_{imf}|}\mathbf{B}_{imf}\right\| \end{cases}. \quad (1)$$

2.6 Reconstruction of the spatial profiles

The following paragraph explains the data processing specific to this study.

2.6.1 Reconstructed profiles through the subsolar magnetosheath

The first goal of this study is to characterize the spatial variation of the magnetic field amplitude and plasma density across the subsolar magnetosheath. This region is of particular interest due to the dominant component of the flow along the Sun–Earth line, which transports magnetic field lines directly from the bow shock to the magnetopause. Our working definition of the subsolar region is the cylinder enclosing all measurements made in a radius of 5 Re $\left(\sqrt{Y_{\mathrm{SWI}}^2 + Z_{\mathrm{SWI}}^2} \leq 5\mathrm{Re}\right)$ spanning the magnetosheath from the shock to the magnetopause, whose

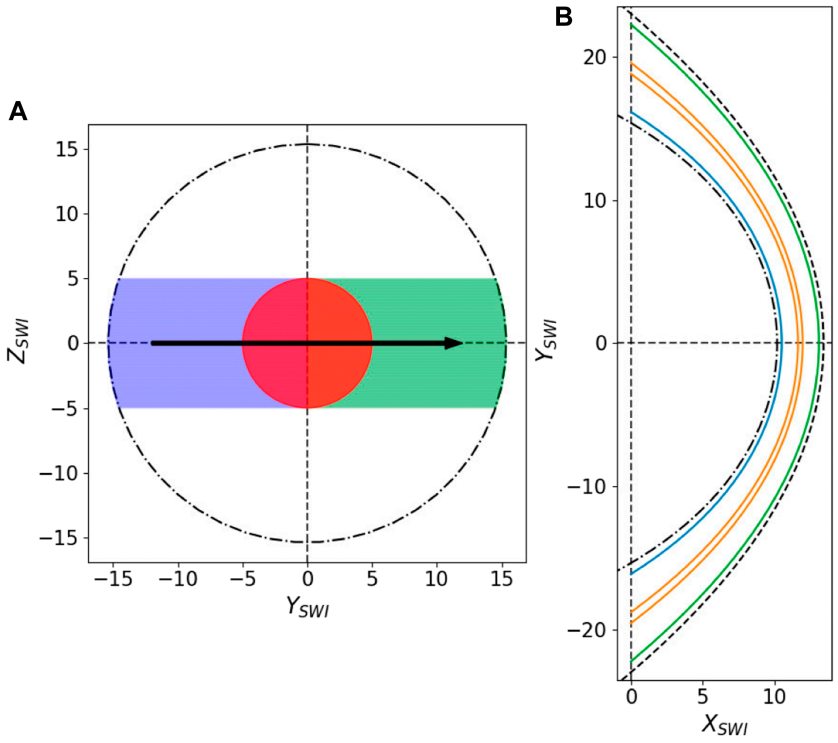

FIGURE 2
(A) Magnetopause terminator (dash-dotted line) viewed from the YZ plane in the SWI coordinate system. The dotted meridian at $Y_{SWI} = 0$ separates the quasi-parallel side ($Y_{SWI} > 0$) from that of the quasi-perpendicular. The green (resp. blue) area spans $10R_e$ around the equator and corresponds to quasi-parallel (resp. quasi-perpendicular) thickness, over which measurements are averaged when investigating the magnetosheath asymmetry in Section 4. The red disk corresponds to the projection of the subsolar cylinder, within which measurements are averaged for each relative position D_{msh} along the Sun–Earth line. The black arrow shows the direction of the IMF in the SWI frame. **(B)** SWI equatorial cut through the system. The dash dot and dashed line represent the magnetopause and bow shock, respectively. The blue line marks the relative radial position $D_{msh} = 0.1$. The orange lines delimit a band in the central magnetosheath of thickness $\Delta D_{MSH} = 0.1$. The green line marks the relative radial position $D_{msh} = 0.9$.

projection is represented as the red area depicted in the left panel of Figure 2.

The variations in the magnetic field amplitude and density are examined with respect to the position D_{msh} in the magnetosheath relative to the magnetopause and the bow shock, defined in Eq. 2, where R, R_{mp}, and R_{bs} correspond to the radial positions of the data point, magnetopause, and bow shock, respectively. The bins are spaced by $\Delta D_{msh} = 0.025$, and the value attributed to each bin corresponds to the median of all the data points within a distance of 0.05. In addition, we will study the variation in the magnetic field and density near the magnetopause ($D_{\mathrm{msh}} \leq 0.1$) as a function of both the IMF cone and clock angle. The supplementary material contains information about the standard deviation of the magnetic field amplitude and plasma density, as well as figures regarding the sample size per bin.

$$D_{\mathrm{msh}} = \frac{R - R_{\mathrm{mp}}}{R_{\mathrm{bs}} - R_{\mathrm{mp}}}. \tag{2}$$

2.6.2 Asymmetries between the quasi-parallel and quasi-perpendicular sides

The SWI coordinate system (see Section 2.5) is particularly useful for studying the asymmetries between the quasi-parallel and quasi-perpendicular sides of the magnetosheath.

We estimate the asymmetry, hereafter denoted as A, of a quantity Q (either magnetic field amplitude or plasma density) within the magnetosheath using Eq. 3. This asymmetry is evaluated between the quasi-perpendicular and quasi-parallel regions as a function of Y_{SWI}. Positive values of asymmetry A signify higher values of the quantity Q on the quasi-perpendicular side of the magnetosheath, represented by the blue area in Figure 2, left panel. Conversely, negative A indicates higher values of the quantity Q on the quasi-parallel side of the magnetosheath, represented by the green shaded area of the same figure. For simplicity and to illustrate the point effectively, we will focus on estimating the asymmetry in the equatorial plane, defined here as measurements satisfying $|Z_{\mathrm{SWI}}| \leq 5$.

$$A\left(Y_{\mathrm{SWI}}\right) = 100\left(\frac{Q\left(-Y_{\mathrm{SWI}}\right)}{Q\left(Y_{\mathrm{SWI}}\right)} - 1\right) \quad \text{with} \quad Y_{\mathrm{SWI}} \geq 0. \tag{3}$$

This study will examine the asymmetry of the magnetic field and density within the magnetosheath at three distinct relative distances: near the magnetopause ($D_{\mathrm{msh}} \leq 0.1$), at the center of the magnetosheath ($0.45 \leq D_{\mathrm{msh}} \leq 0.55$), and close to the bow shock ($D_{\mathrm{msh}} \geq 0.9$). These regions are illustrated in the right panel of Figure 2. Additionally, the variation in the asymmetry throughout the magnetosheath will be studied by averaging it over all Y_{SWI} for different relative distances from the shock to the magnetopause.

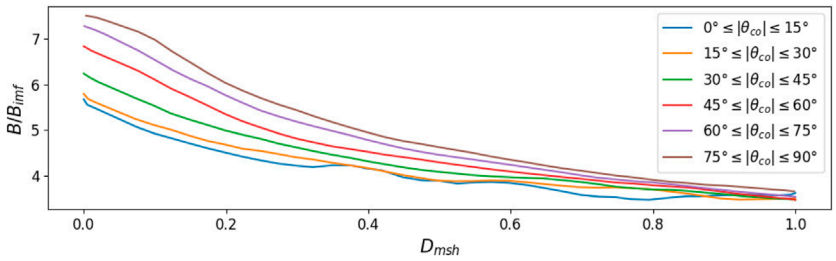

FIGURE 3
Magnetic field amplitude in the subsolar magnetosheath $\left(\sqrt{Y_{SWI}^2 + Z_{SWI}^2} \leq 5R_e\right)$ normalized by the IMF amplitude (B_{imf}) as a function of the position in the magnetosheath D_{msh} relative to the magnetopause and bow shock. The magnetopause and bow shock are positioned at D_{msh} = 0 and D_{msh} = 1, respectively. The different colored lines represent the compression of the magnetic field for different absolute value of IMF cone angles ($|\theta_{co}|$).

3 Magnetic amplitude and plasma density through the subsolar magnetosheath

3.1 Variability in the magnetic pileup with the IMF orientation

Figure 3 presents the profile of the magnetic field amplitude as a function of the relative position D_{msh} across the subsolar magnetosheath for various IMF cone angles $|\theta_{co}|$. The plot reveals the presence of a monotonous increase in the magnetic amplitude across the magnetosheath, whatever the value of the IMF cone angles, resulting from the global magnetic flux pileup against the magnetosphere obstacle. We also distinctly observe that the pileup becomes more pronounced as the IMF cone angle increases. Close to the magnetopause, the magnetic field amplitude in radial IMF conditions is lower by an offset of approximately $2B_{imf}$. Downstream of the shock, the magnetic field amplitude shows relatively similar values for all IMF cone angles.

As demonstrated by Michotte de Welle et al. (2022), the IMF cone angle has a significant influence on how the magnetic field drapes around the magnetopause. A key factor regarding how it also affects the field amplitude is that as the IMF becomes increasingly radial, it also becomes more aligned with the solar wind bulk velocity. The perpendicular component of the magnetosheath flow is geometrically smaller, thereby diminishing the rate at which magnetic flux is brought to the magnetopause boundary. Magnetic flux thus has more time to get around the obstacle without having to pile up against it, leading to overall smaller field amplitudes.

The behavior of the magnetic field is completely different when considering the impact of the IMF clock angle. Figure 4 shows the profile of the magnetic field amplitude as a function of D_{msh} in the subsolar region for various IMF clock angles $|\theta_{cl}|$. As stated previously, it is immediately visible that the magnetic field amplitude increases from the bow shock to the magnetopause, whatever the value of the IMF clock angle. However, and in contrast to the behavior observed when varying the IMF cone angle, the amplitude of the magnetic field stays remarkably independent of the IMF clock angle from the bow shock up to the last 40% of the magnetosheath. A dependence on the IMF clock angle is only visible in the last 40% of the magnetosheath, and it grows when approaching the magnetopause. Near the magnetopause, the magnetic pileup increases as the IMF clock angles decrease, with a difference of B/B_{imf} of approximately 1 at the boundary between the most northward and southward IMF conditions. Interestingly, the decrease in the magnetic pileup when the IMF turns from a northward to a southward direction is not linear with the clock angle but rather abruptly changes for IMF clock angles greater than 60° ($|\theta_{cl}| \geq 60°$). This nonlinear transition distinguishes northward IMF conditions, with $|\theta_{cl}| \leq 60°$, from southward IMF conditions ($|\theta_{cl}| \geq 90°$), where the magnetic field amplitudes remain relatively similar. Only a slight decrease in the magnetic amplitude is seen when the IMF clock angle changes from 90° to 180°.

The decrease in the flux pileup effect with increasing IMF clock angles is consistent with magnetic reconnection operating at the magnetopause with increasing efficiency. While the IMF is still northward for the 60° clock angle, the sharp transition observed in the amount of pileup could result from the transition of the X line from high latitudes to a tilted dayside configuration. Figure 5 shows the V_x component of the ion bulk velocity across the subsolar magnetosheath from the bow shock to the magnetopause, normalized by the solar wind velocity V_{sw}. As for the magnetic amplitude, this spatial profile is shown for different values of the IMF clock angle. Overall, the velocity is seen to linearly decrease up to the magnetopause, as expected from plasma piling-up against the obstacle. We also note that the velocity increases with the IMF clock angle, and this occurs throughout the whole thickness of the magnetosheath. This larger flow along the Sun–Earth line for more southward conditions is, again, consistent with reconnection operating at the magnetopause in these conditions. Reconnection barely occurs, if at all, around the due north IMF conditions. As a result, the plasma flow in the magnetosheath, decelerated downstream of the bow shock, must globally be consistent with a closed magnetopause boundary condition, imposing a purely tangential flow there. In such a regime, magnetic flux and plasma pile up against the obstacle more as the only way out stands in being deflected radially from the subsolar point toward the flanks of the system. In contrast, as soon as reconnection is enabled at the magnetopause, the whole flow adjusts to the now open boundary condition at the magnetopause, acting as a new sink and essentially allowing larger transport along the Sun–Earth line. Considering $V_{sw} \approx 400\ km/s$, the offset in the velocity seen between the due north and due south IMF is approximately 10 km/s, which is consistent with the expected subsolar reconnection inflow.

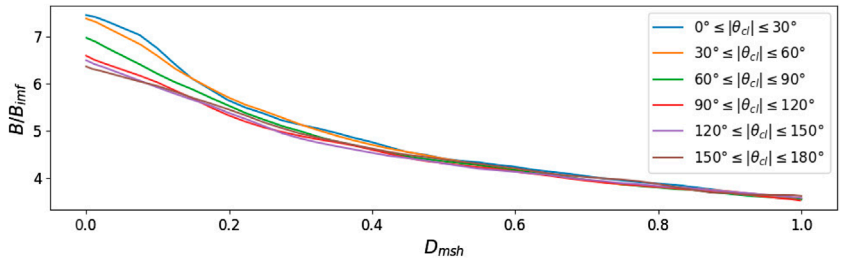

FIGURE 4
Magnetic field amplitude in the subsolar magnetosheath $\left(\sqrt{Y_{SWI}^2 + Z_{SWI}^2} \leq 5Re\right)$ normalized by the IMF (B_{imf}) as a function of the position in the magnetosheath D_{msh} relative to the magnetopause and bow shock. The magnetopause and bow shock are positioned at D_{msh} = 0 and D_{msh} = 1, respectively. The different colored lines represent the compression profiles of the magnetic field for different absolute value of IMF clock angles ($|\theta_{cl}|$).

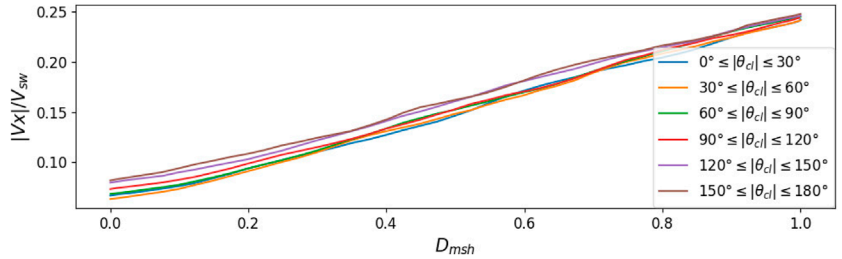

FIGURE 5
Profiles of the Vx component of the velocity in the subsolar magnetosheath $\left(\sqrt{Y^2 + Z^2} \leq 5Re\right)$ normalized by the solar wind velocity as a function of the position in the magnetosheath D_{msh} relative to the magnetopause and bow shock. The magnetopause and bow shock are positioned at D_{msh} = 0 and D_{msh} = 1, respectively. The different colored lines represent the Vx component for different absolute values of IMF clock angles ($|\theta_{cl}|$).

Let us now focus on how the magnetic field amplitude values vary as a function of both the IMF clock and cone angles, but only near the subsolar magnetopause. Figure 6 shows the values taken by the normalized magnetic field in the subsolar region near the magnetopause ($D_{msh} \leq 0.1$) as a function of both the IMF clock and cone angles. Overall, the observed variation in magnetic amplitude, ranging from approximately 5 in the southward and low IMF cone angle to approximately 8.5 (i.e. 70% increase) in the northward and large cone angle conditions, supports previous findings. We can also see that for IMF cone angles smaller than 20°, the magnetic pileup does not appear to decrease as the IMF turns southward. This may suggest that, for such a low IMF cone angle, magnetic reconnection may not be operating at the magnetopause, or it may be so small that it does not impact how the magnetic field piles up. In contrast, for IMF cone angles greater than 60°, the magnetic pileup decreases rapidly when the IMF clock angle is between 60° and 90°, and it appears to be almost constant for more southward IMF. For such values of IMF cone angle, the magnetic field strength for northward IMF is approximately 30% greater than that for southward IMF.

3.2 Magnetosheath plasma density and depletion layer for various IMF orientations

We repeat the same procedure as in previous sections, but this time focusing on plasma density across the magnetosheath, particularly investigating the possible depletion layer near the magnetopause. We start by investigating the particle density profile as a function of the relative position across the subsolar magnetosheath for different IMF cone angles, considering all clock angles, as shown in Figure 7.

Near the bow shock, the density ratio increases with increasing IMF cone angle, reaching a maximum compression of approximately 4 when the IMF is almost perpendicular to the shock ($|\theta_{co}| \geq 60°$).

For the most radial IMF conditions ($|\theta_{co}| \leq 30°$), the density ratio exhibits an almost continuous increase up to the magnetopause, where no depletion is observed. In contrast, a PDL near the magnetopause is observed for IMF with cone angles greater than 30°. The density ratios increase up to approximately $D_{msh} = 0.4$ ($\approx 1.2\ R_e$ along the subsolar magnetosheath), after which they decrease up to the magnetopause. Interestingly, for IMF cone angles greater than 60°, the density ratio at the magnetopause is even lower than that at the bow shock. The magnitude of the depletion of plasma near the magnetopause increases with the IMF cone angle. This is consistent with the concomitant increase in the magnetic field amplitude seen in Figure 3 and has been previously discussed. It is important to note that at this point, in contrast to the findings of Zhang et al. (2019), the density depletion we observe close to the magnetopause cannot, by construction, result from mispositioning measurements made in the magnetosphere since those are excluded from the original dataset.

Similarly to our investigation of the magnetic amplitude, we now investigate how the density profile changes for different IMF clock angles. Figure 8 presents the density profile as a function of

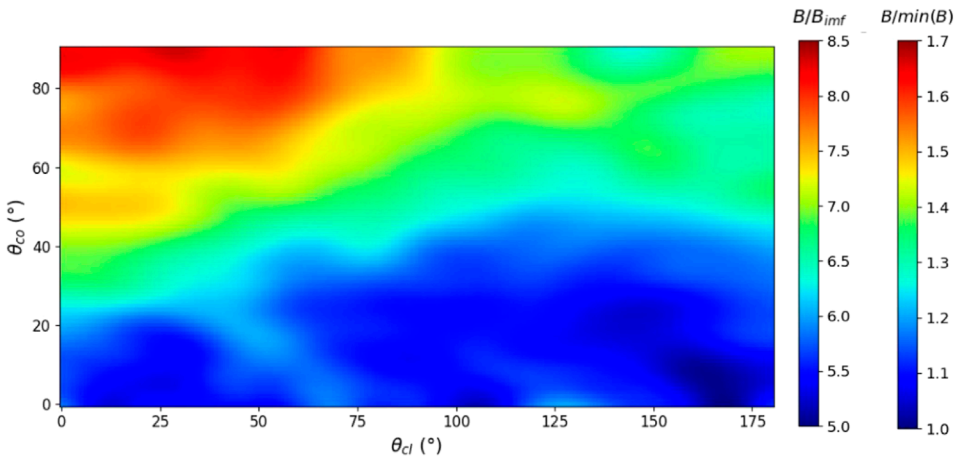

FIGURE 6
Magnetic pileup (B/B_{imf}) near the magnetopause ($D_{msh} \leq 0.1$) in the subsolar magnetosheath $\left(\sqrt{Y^2+Z^2} \leq 5\text{Re}\right)$ as a function of the IMF clock ($|\theta_{cl}|$) and cone ($|\theta_{co}|$) angles. The two color bars provide the magnetic field amplitude in the magnetosheath, normalized by the IMF strength, and the minimum value of the magnetic field amplitude ratio, respectively.

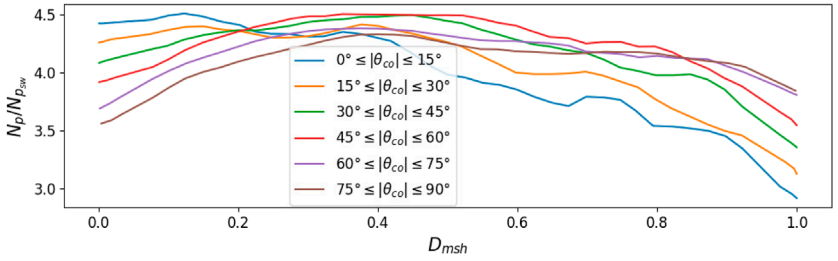

FIGURE 7
Ion density ratio ($N_p/N_{p_{sw}}$) in the subsolar magnetosheath $\left(\sqrt{Y^2+Z^2} \leq 5\text{Re}\right)$ as a function of the position in the magnetosheath D_{msh} relative to the magnetopause and bow shock. The magnetopause and bow shock are positioned at $D_{msh} = 0$ and $D_{msh} = 1$, respectively. The different colored lines represent the profiles of the plasma density for different absolute value of IMF cone angles ($|\theta_{co}|$).

the relative positionD_{msh} throughout the subsolar magnetosheath for various IMF clock angles θ_{cl}. We observe a PDL for each of the IMF clock angles, and there is no clear dependence on the IMF clock angle throughout most of the magnetosheath. Near the magnetopause ($D_{msh} \leq 0.2$), however, the density appears to be lower for small IMF clock angles. The deepening of the depletion seems to predominantly occur as soon as the IMF clock angle passes 60°. This pattern is consistent with the observed increase in magnetic pileup, as shown in Figure 4. Together, the magnetic field amplitude and plasma density, in their dependence on the IMF clock angle, seem to be consistent with magnetic reconnection eroding the pileup and the PDL as the IMF turns southward.

Let us now focus on the region near the magnetopause and observe in more detail how the density varies with both the IMF cone and clock angles. Figure 9 shows the density ratio in the subsolar region close to the magnetopause ($D_{msh} \leq 0.1$) as a function of both the IMF clock and cone angles. The density ratio decreases as the IMF cone angle increases, with depletion of plasma between 30%from small to large cone angles and northward IMF. Consistent with the magnetic field amplitude (Figure 6), the density does not seem to have a clear dependence on the IMF clock angle for IMF cones under 20°. The density ratio is the smallest for northward IMF ($|\theta_{cl}| \leq 25°$) at large IMF cone angles ($|\theta_{co}| \geq 45°$), where the magnetic pileup is maximum. In contrast, as the IMF turns southward, its value rapidly increases. Once the IMF becomes eastward ($|\theta_{cl}| \geq 60°$), the density values do not seem to exhibit a strong dependence on the IMF clock angle but only on the IMF cone angle. Overall, the observed variation in the density ratio is consistent with the variation in the magnetic field and the effect of magnetic reconnection.

4 Asymmetry of the equatorial magnetosheath

4.1 Asymmetry of the magnetic field amplitude

The first part of this work focused on the state of the magnetosheath along the Sun–Earth line. We now focus on the longitudinal variations and, more specifically, on the asymmetries that may develop along that dimension. Previous studies investigating the amount of asymmetry in the dayside magnetosheath either looked at the asymmetries integrated

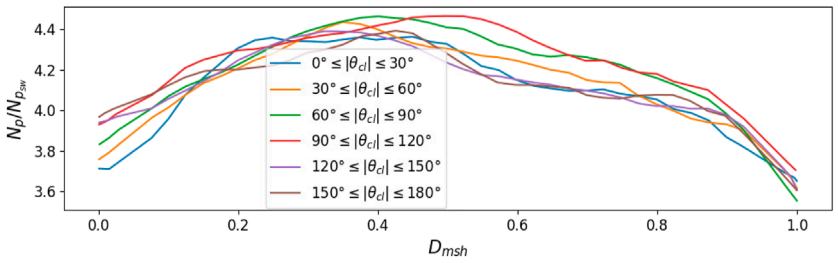

FIGURE 8
Ion density ratio ($N_p/N_{p_{sw}}$) in the subsolar magnetosheath $\left(\sqrt{Y^2+Z^2} \leq 5\text{Re}\right)$ as a function of the position in the magnetosheath D_{msh} relative to the magnetopause and bow shock. The magnetopause and bow shock are positioned at $D_{msh} = 0$ and $D_{msh} = 1$, respectively. The different colored lines represent the profiles of the plasma density for different absolute value of IMF clock angles ($|\theta_{cl}|$).

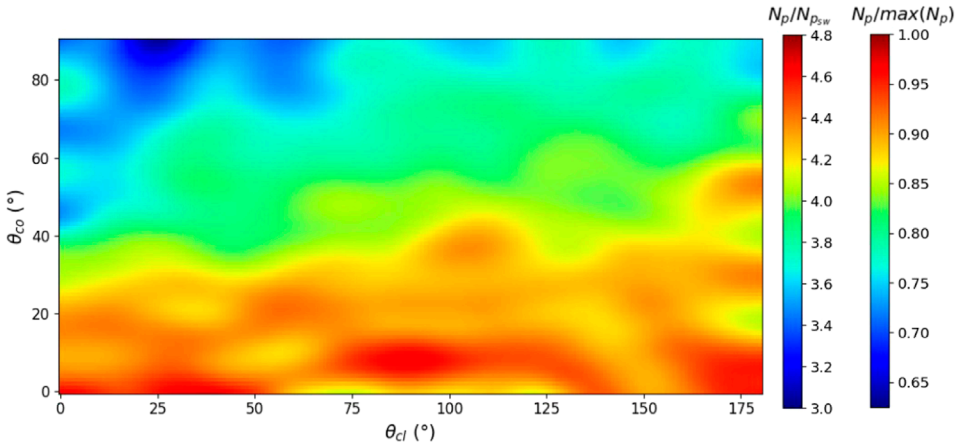

FIGURE 9
Density ratio ($N_p/N_{p_{sw}}$) near the magnetopause ($D_{msh} \leq 0.1$) in the subsolar magnetosheath $\left(\sqrt{Y^2+Z^2} \leq 5\text{Re}\right)$ as a function of the IMF clock ($|\theta_{cl}|$) and cone ($|\theta_{co}|$) angles. The two color bars provide the plasma density in the magnetosheath, normalized by the solar wind density, and the maximum value of the density ratio, respectively.

through the whole magnetosheath thickness or those close to the magnetopause only. By covering the whole dayside magnetosheath volume, our dataset presents an interesting opportunity to get more local insight into the asymmetries. Thus, in this study, we will consider how the asymmetry also varies with the depth within the magnetosheath, from the bow shock to the magnetopause.

Figure 10 presents the amplitude of the magnetic field (left panels) along the Y_{SWI} direction in the equatorial magnetosheath. The right panels show the associated asymmetry in the magnetic amplitude, as calculated from Eq. 3. These profiles are made close to the magnetopause, in the middle of the magnetosheath, close to the bow shock, and for varying IMF cone angles.

For IMF cone angles greater than 80° ($|\theta_{co}| \geq 80°$), panel a reveals no significant asymmetry in the magnetic field for any magnetopause distance. The corresponding asymmetry on panel b confirms the rather symmetric configuration, with values close to zero across the magnetosheath. If the IMF is the main underlying source of asymmetry, this lack of asymmetry is expected since for such a large IMF cone angle, there is essentially no side that is more quasi-parallel than the other.

An asymmetry starts to be visible for IMF cone angles of $50° \leq |\theta_{co}| \leq 60°$, corresponding approximately to the Parker spiral orientation. Panel c shows an asymmetry from the bow shock to the middle magnetosheath, with slightly larger magnetic amplitudes on the quasi-perpendicular side of the magnetosheath. However, the asymmetry seems to have almost disappeared near the magnetopause, where the amplitude is the strongest. Panel d shows that the asymmetry is relatively similar near the bow shock and in the middle of the magnetosheath, increasing from the subsolar region to the terminator ($X_{SWI} = 0$), reaching values of approximately 20% higher in the quasi-perpendicular side. Near the magnetopause, the asymmetry shows significant variability and is perhaps a little positive in the quasi-perpendicular region, if not zero.

For IMF cone angles of $20° \leq |\theta_{co}| \leq 30°$, panel e reveals higher values in the magnetic field on the quasi-perpendicular side throughout the magnetosheath thickness. The asymmetry, shown on panel f, reveals that the asymmetry near the shock and in the middle of the magnetosheath increases from the subsolar region to the terminator similarly. At the terminator, it reaches approximately 30% higher values in favor of the quasi-perpendicular side. In contrast, the asymmetry near the magnetopause appears to remain relatively constant, with the quasi-perpendicular side exhibiting magnetic field values of approximately 10% stronger.

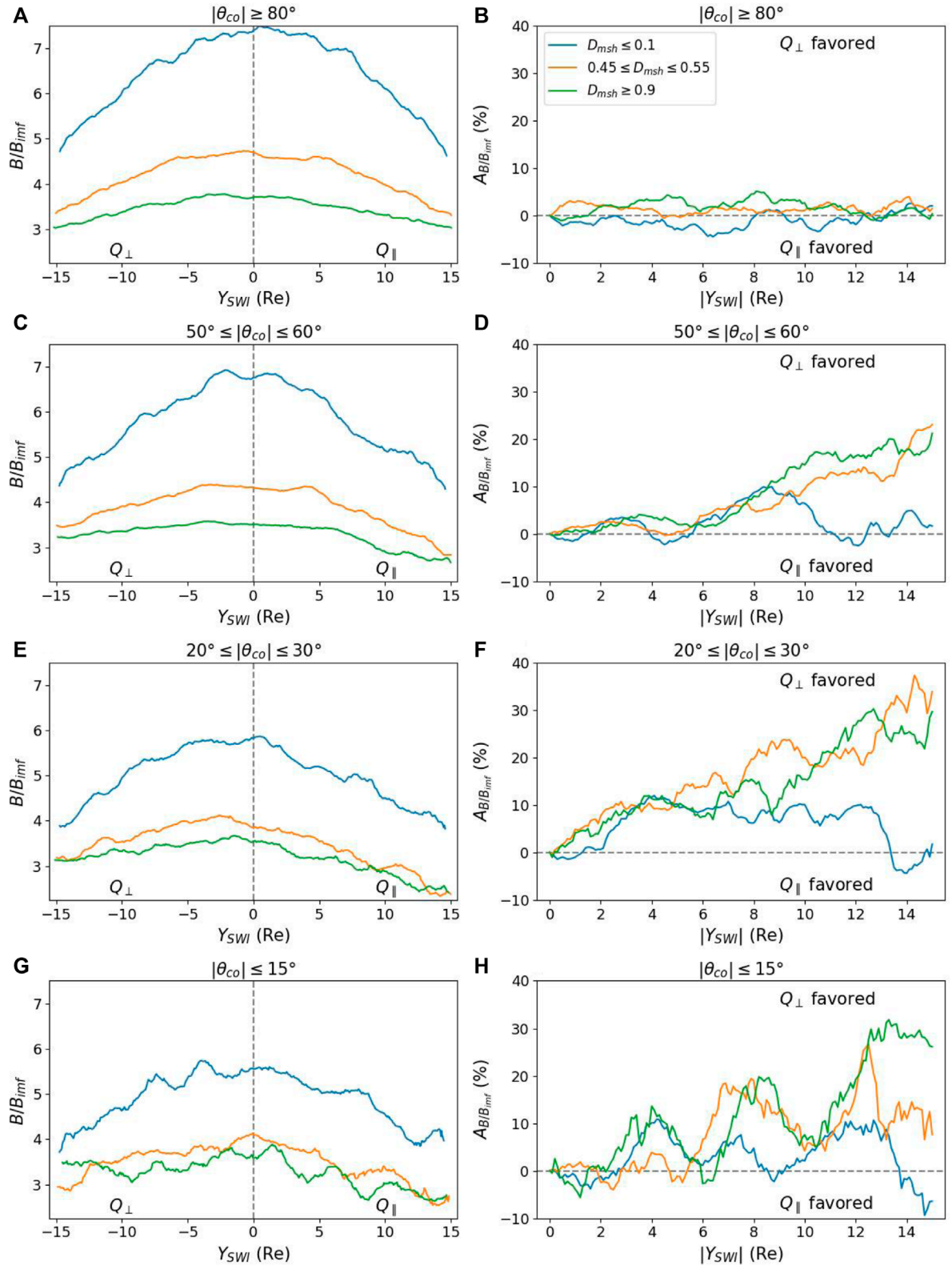

FIGURE 10
Left panels show the distribution of the magnetic field amplitude as a function of Y_{SWI}. The right panels show the asymmetry $A(B/B_{imf})$ (Eq. 3) between the quasi-parallel and quasi-perpendicular side of the magnetosheath. The top, second, third, and last rows correspond to IMF cone angles of $|\theta| \geq 80°$, $50° \leq |\theta| \leq 60°$, $20° \leq |\theta| \leq 30°$, and $|\theta| \leq 15°$, respectively. The green, orange, and blue lines correspond to the magnetic field amplitude or asymmetry near the bow shock ($D_{msh} \geq 0.9$), at the center of the magnetosheath ($0.45 \leq D_{msh} \leq 0.55$), and near the magnetopause ($D_{msh} \leq 0.1$), respectively. $Q_\parallel$ and $Q_\perp$ stand for the quasi-parallel and quasi-perpendicular side of the magnetosheath, respectively.

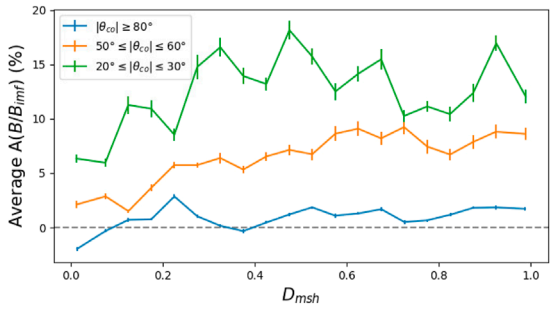

FIGURE 11
Average asymmetry $A(B/B_{imf})$ (Eq. 3) in the magnetic field amplitude between the quasi-parallel and quasi-perpendicular as a function of the magnetosheath distance (D_{msh}).

Finally, for IMF cone angles of $|\theta_{co}| \leq 15°$, panel g shows slightly higher values on the quasi-perpendicular side of the magnetosheath from the shock to the magnetopause, which is confirmed in the asymmetry of panel h. As the IMF becomes almost radial, it is expected that the asymmetry will decrease. The lack of radial IMF measurements and the presence of the foreshock result in a relatively noisy asymmetry.

The asymmetry is not uniform from the shock to the magnetopause. To get a clearer vision of the dependence on the depth in the magnetosheath, we can compute the asymmetry as previously for many different depth shells and plot the average asymmetry per shell. The result is shown in Figure 11, where the average asymmetry in the magnetic field amplitude between the quasi-parallel and quasi-perpendicular sides in the equatorial region as a function of the distance in the magnetosheath thickness (D_{msh}) is plotted. For IMF cone angles greater than 80° ($|\theta| \geq 80°$), the average asymmetry remains relatively constant, with values close to zero, indicating a lack of distinct asymmetry throughout the magnetosheath. For IMF cone angles between 50° and 60° ($50° \leq |\theta| \leq 60°$), the average asymmetry indicates that the quasi-perpendicular side of the magnetosheath has a higher value of approximately 8% from the shock to the middle of the magnetosheath, and then it decreases to 2.5% near the magnetopause. For IMF cone angles between 20° and 30° ($20° \leq |\theta| \leq 30°$), the average asymmetry remains relatively constant throughout most of the magnetosheath, with values approximately 15% higher on the quasi-perpendicular side. However, this asymmetry decreases closer to the magnetopause ($D_{msh} \leq 0.2$) to approximately 6%.

Overall, the asymmetry in the magnetic field amplitude between the quasi-perpendicular and quasi-parallel sides of the magnetosheath decreases as the IMF cone angle increases and presents smaller values at the magnetopause compared to the rest of the magnetosheath. It should be noted that no clear effect of the IMF clock angle on the magnetic field asymmetry was observed.

4.2 Asymmetry in the plasma density

Figure 12 presents the ratio of the plasma density and its asymmetry between the quasi-parallel ($Y_{SWI} \geq 0$) and quasi-perpendicular ($Y_{SWI} \leq 0$) sides of the equatorial region of the magnetosheath.

For all IMF cone angles (left panels), the density in the flanks ($|Y_{SWI}| \geq 5$ Re) at the magnetopause is smaller than that in the center of the magnetosheath, indicating the presence of a PDL in these regions. Interestingly, the presence of these flank PDLs seems to be relatively independent of the magnetic field amplitude and IMF cone angle.

For IMF cone angles greater than 80° ($|\theta_{co}| \geq 80°$), the normalized density values are highest in the middle of the magnetosheath and smaller near the magnetopause than near the bow shock, confirming for different Y positions what was already observed in the subsolar region in Figure 7. The profiles do not show any asymmetries between the quasi-parallel and quasi-perpendicular sides of the magnetosheath. This is confirmed in the corresponding asymmetry plot (panel b), where the values remain close to zero from the shock to the magnetopause. The absence of asymmetry in the density for such IMF cone angles is consistent with the lack of asymmetry observed in the magnetic field amplitude (upper panels of Figure 10).

For IMF cone angles between 50° and 60° ($50° \leq |\theta_{co}| \leq 60°$), the normalized density (panel c) is slightly higher in the subsolar magnetopause than near the bow shock, while remaining maximum in the middle of the magnetosheath, which is again consistent with Figure 7. The normalized density profile in the equatorial region does not exhibit a clear asymmetry between the quasi-perpendicular and quasi-parallel sides of the magnetosheath near the bow shock. However, at greater depth, in the center of the magnetosheath and near the magnetopause, the quasi-parallel side shows higher values than the quasi-perpendicular side. In panel d, the values of the asymmetry near the bow shock vary around zero, indicating no distinct asymmetry in this region. In contrast, in the center of the magnetosheath and near the magnetopause, the asymmetry increases from the subsolar region to the terminator, reaching values approximately 15% higher in the quasi-parallel side, which is consistent with results obtained by Walsh et al. (2012); Dimmock et al. (2016). Note that in contrast to the magnetic field (panels c and d of Figure 10), the asymmetry in the normalized density seems to increase from the shock to the magnetopause.

Panel e shows the density profile for IMF cone angles between 20° and 30° ($20° \leq |\theta_{co}| \leq 30°$). The density near the bow shock shows higher values on the quasi-perpendicular side than on the quasi-parallel side of the magnetosheath. In contrast, in the middle of the magnetosheath, this asymmetry seems to have disappeared, and near the magnetopause, the asymmetry seems to have shifted in favor of the quasi-parallel side, as in the larger IMF cone angle interval. This reversal of the asymmetry is shown clearly in panel f. Near the bow shock side, the density values are approximately 10% higher on the quasi-perpendicular side than on the quasi-parallel. Conversely, near the magnetopause, the density ratio, while being more variable, is approximately 10% higher on the quasi-parallel side of the magnetosheath. In between, no clear asymmetry is distinguishable in the middle of the magnetosheath. The smaller density observed on the quasi-perpendicular side, close to the magnetopause, can be understood as a deeper PDL associated with the stronger magnetic field therein. In contrast, it is unclear why the density is more pronounced on the quasi-perpendicular side just downstream of the bow shock in such low IMF cone angle conditions. Isotropic MHD jump conditions (Zwan and Wolf, 1976) predict higher density on the quasi-parallel side, but a straight comparison with our observations, averaged over all Mach and

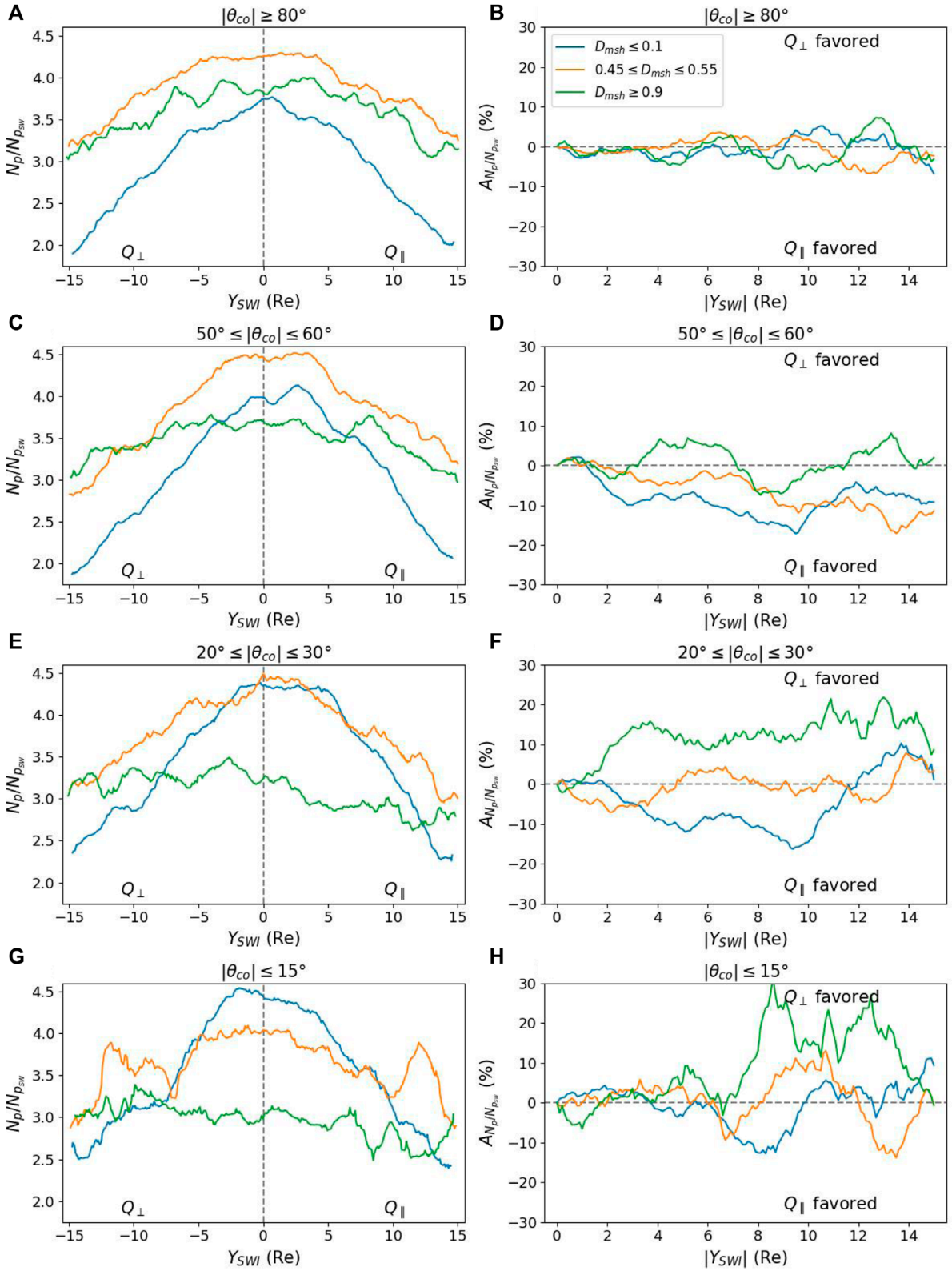

FIGURE 12
Left panels shows the distribution of the density ratio as a function of Y_{SWI}. The right panels show the asymmetry $A(N_p/N_{p_{sw}})$ (Eq. 3) between the quasi-parallel and quasi-perpendicular side of the magnetosheath. The top, second, third, and last rows correspond to IMF cone angles of $|\theta| \geq 80°$, $50° \leq |\theta| \leq 60°$, $20° \leq |\theta| \leq 30°$, and $|\theta| \leq 15°$, respectively. The green, orange, and blue lines correspond to the magnetic field amplitude or asymmetry near the bow shock ($D_{msh} \geq 0.9$), at the center of the magnetosheath ($0.45 \leq D_{msh} \leq 0.55$), and near the magnetopause ($D_{msh} \leq 0.1$), respectively. $Q_\parallel$ and $Q_\perp$ stand for the quasi-parallel and quasi-perpendicular side of the magnetosheath, respectively.

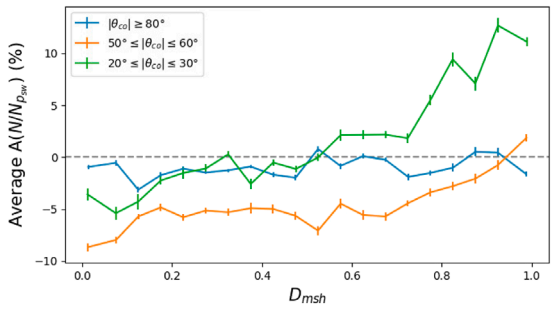

FIGURE 13
Average asymmetry $A(N_p/N_{p_{sw}})$ (Eq. 3) in the plasma density between the quasi-parallel and quasi-perpendicular as a function of the magnetosheath distance (D_{msh}).

relevant shock parameters, is not possible; in addition, such MHD approximations are questionable downstream of quasi-parallel shock, where turbulence and instabilities play an important role.

Finally, for IMF cone angles of $|\theta_{co}| \leq 15°$, panel g shows slightly higher density values on the quasi-parallel side of the magnetosheath in proximity to the shock. However, there is no clear asymmetry between the quasi-parallel and quasi-perpendicular sides in the middle of the magnetosheath and close to the magnetopause (panel h).

Figure 13 presents the asymmetry in the normalized density between the quasi-parallel and quasi-perpendicular sides in the equatorial region, averaged over Y_{SWI}, and as a function of the position D_{msh} throughout the magnetosheath. For IMF cone angles greater than 80° ($|\theta_{co}| \geq 80°$), the average asymmetry remains relatively constant, with values close to zero, indicating a lack of distinct asymmetry throughout the magnetosheath. For IMF cone angles between 50° and 60° ($50° \leq |\theta_{co}| \leq 60°$), the average asymmetry decreases from the values close to zero in proximity of the bow shock to approximately −8% near the magnetopause, indicating that the plasma density is larger on the quasi-parallel side than on the quasi-perpendicular side of the magnetosheath. For IMF cone angles between 20° and 30° ($20° \leq |\theta_{co}| \leq 30°$), the average asymmetry decreases from approximately 10% (i.e., higher density on the quasi-perpendicular side) to −5% (i.e., higher density on the quasi-parallel side) from the shock to the magnetopause. As mentioned above, this reversal of the density asymmetry between the quasi-perpendicular and quasi-parallel sides of the magnetosheath is attributed to the combined effects of the bow shock and magnetic pileup.

It should be noted that similar to the magnetic field, no clear effect of the IMF clock angle on the density asymmetry was observed.

5 Discussion and conclusion

The magnetosheath is the region where the solar wind and interplanetary magnetic field are altered before coming into contact with the magnetopause. Its characterization, therefore, constitutes a primary objective in understanding how the Earth magnetosphere couples with its surrounding environment. Despite decades of measurements, the spatial structure of macroscopic parameters such as density and magnetic field, which primarily control how reconnection occurs at the magnetopause, remains poorly understood. By using a comprehensive dataset based on decades of multi-mission measurements, we have, in this study, proposed to explore the spatial distributions of the plasma density and magnetic field amplitude and their functional dependence on the IMF orientation. The magnetic field pileup against the magnetopause and the subsequent monotonous increase in the magnetic amplitude throughout the magnetosheath are general properties of the system. The pileup is shown to be less pronounced as the IMF becomes increasingly aligned with the Sun–Earth axis, as expected from the smaller rate at which magnetic flux is carried against the obstacle. The dependence on the IMF clock angle is more subtle and only appears clearly in the first 40% of the magnetosheath from the magnetopause. The strength of the magnetic pileup decreases non-linearly as the IMF turns to the south, which is consistent with the expected effect of magnetic reconnection occurring at the magnetopause. As for the magnetic field, the plasma density profile in the subsolar magnetosheath strongly depends on how radial the IMF is. Except for the most radial IMF orientations, a plasma depletion layer is generally observed in the first 40% of the magnetosheath from the magnetopause. The depth of the PDL increases as the IMF cone angle increases, which is consistent with the observation of a pronounced magnetic flux pileup. It also increases as the IMF clock angle decreases as a result of magnetic reconnection not being able to process incoming magnetic flux as much. The effect of magnetic reconnection has also been shown to be consistently revealed through the faster flow along the Sun–Earth line as the IMF clock angle increases, as expected from an open magnetopause boundary condition to the magnetosheath flow. It should be noted that this study interprets the variations in magnetic field amplitude and plasma density as primarily produced by magnetic reconnection. However, other processes, such as Kelvin–Helmholtz, surface waves, high-speed jets, and others, may alter the density and magnetic amplitude. Nevertheless, we anticipate that their impact will be more localized in space and time and, thus, less or not visible in large-scale statistics such as those presented in this study. The coupling between the depth of the PDL and strength of the magnetic field close to the magnetopause has also been revealed in the longitudinal variations in the quantity in the equatorial magnetosheath. The magnetic field amplitude is slightly higher on the quasi-perpendicular side of the magnetosheath adjacent to the magnetopause, resulting in a deeper PDL and a quasi-parallel favored asymmetry in that region, which is consistent with previous studies. Interestingly, we showed that the density adjacent to the magnetopause can even become smaller than downstream of the bow shock despite the overall pileup of the solar wind onto the obstacle. In contrast to previous studies, our spatial reconstruction revealed significant variations in the asymmetries in the magnetic field and density across the thickness of the magnetosheath. The magnetic field amplitude asymmetry, which was rather pronounced and quasi-perpendicularly favored downstream of the bow shock, was shown to be much weaker close to the magnetopause in the pileup region. The asymmetry of the density was shown to even reverse at mid-depth and become quasi-perpendicular favored downstream of the bow shock, particularly in the most radial IMF conditions.

This study revealed the first detailed spatial reconstruction of the plasma density and magnetic field in the magnetosheath. The study, in particular, highlighted the subtle effect of magnetic reconnection at the magnetopause on the extent to which the magnetic flux piles up and the density is subsequently depleted near the magnetopause. Our results clearly show how reconnection at the magnetopause changes the global state of the magnetosheath by changing the innermost boundary condition of the flow. Inversely and interestingly, this also implies that magnetic reconnection non-linearly modifies its own boundary condition.

We believe that the main limitation of this study is the repositioning errors of the data points, which result from a combination of errors in determining SW/IMF and the intrinsic errors of the boundary models themselves. This lack of spatial resolution results in the mixing of the plasma and magnetic structures (i.e., magnetic pileup and PDL), which could exhibit a lesser degree of variation than that observed when examining a temporal crossing of the magnetopause/magnetosheath.

The results of this study open several avenues for future investigations. First, this study examines the state of the magnetosheath primarily through the prism of the IMF orientation. Although this parameter is critically important due to its effect on magnetic reconnection, it is far from the only significant factor. Future works should focus on the dependence on the upstream Mach number and plasma beta as these parameters also significantly alter the properties of the PDL and magnetic reconnection at the magnetopause. Future work should also focus on reconstructing the spatial distribution of other parameters, such as plasma flow and plasma pressure and their anisotropy, and conditioning the development of instabilities, whose signatures (such as mirror structures) could also be spatially mapped in order to assess their effects on magnetopause processes. While they only represent an averaged overview of the global magnetosheath, the spatial reconstructions obtained in our study pave the way for new investigations of the magnetosheath from *in situ* measurements, which were previously accessible only to global numerical models.

Data availability statement

The original contributions presented in the study are included in the article/Supplementary Material; further inquiries can be directed to the corresponding author.

Author contributions

BM: writing–original draft and writing–review and editing. NA: writing–original draft and writing–review and editing. BL: writing–review and editing. VG: writing–review and editing. AJ: writing–review and editing. GN: writing–review and editing. AG: writing–review and editing. RS: writing–review and editing.

Funding

The author(s) declare that financial support was received for the research, authorship, and/or publication of this article. This work was supported by a French government grant managed by the Agence Nationale de la Recherche under the Investissements d'Avenir program (ANR-18-EURE-0014).

Acknowledgments

The authors are grateful to the CDPP/AMDA, CDAWEB, and CSA for the data access. Computing resources used for the data analysis have been funded by the Plasapar federation.

Conflict of interest

The authors declare that the research was conducted in the absence of any commercial or financial relationships that could be construed as a potential conflict of interest.

Publisher's note

Supplementary material

The Supplementary Material for this article can be found online at: https://www.frontiersin.org/articles/10.3389/fspas.2024.1427791/full#supplementary-material

References

Anderson, B. J., and Fuselier, S. A. (1993). Magnetic pulsations from 0.1 to 4.0 Hz and associated plasma properties in the Earth's subsolar magnetosheath and plasma depletion layer. *J. Geophys. Res.* 98, 1461–1479. doi:10.1029/92JA02197

Anderson, B. J., Phan, T. D., and Fuselier, S. A. (1997). Relationships between plasma depletion and subsolar reconnection. *J. Geophys. Res.* 102, 9531–9542. doi:10.1029/97JA00173

Auster, H. U., Glassmeier, K. H., Magnes, W., Aydogar, O., Baumjohann, W., Constantinescu, D., et al. (2008). The THEMIS fluxgate magnetometer. *Space Sci. Rev.* 141, 235–264. doi:10.1007/s11214-008-9365-9

Balogh, A., Carr, C., Acuña, M., Dunlop, M., Beek, T., Brown, P., et al. (2001). The cluster magnetic field investigation: overview of in-flight performance and initial results. *Ann. Geophys.* 19, 1207–1217. doi:10.5194/angeo-19-1207-2001

Borovsky, J. E., Hesse, M., Birn, J., and Kuznetsova, M. M. (2008). What determines the reconnection rate at the dayside magnetosphere? *J. Geophys. Res. Space Phys.* 113, A07210. doi:10.1029/2007JA012645

Cairns, I. H., and Fuselier, S. A. (2017). The plasma depletion layer beyond the heliopause: evidence, implications, and predictions for voyager 2 and new horizons. *Astrophysical J.* 834, 197. doi:10.3847/1538-4357/834/2/197

Carr, C., Brown, P., Zhang, T. L., Gloag, J., Horbury, T., Lucek, E., et al. (2005). The Double Star magnetic field investigation: instrument design, performance and highlights of the first year's observations. *Ann. Geophys.* 23, 2713–2732. doi:10.5194/angeo-23-2713-2005

Cassak, P. A., and Shay, M. A. (2007). Scaling of asymmetric magnetic reconnection: general theory and collisional simulations. *Phys. Plasmas* 14, 102114. doi:10.1063/1.2795630

Cooling, B. M. A., Owen, C. J., and Schwartz, S. J. (2001). Role of the magnetosheath flow in determining the motion of open flux tubes. *J. Geophys. Res.* 106, 18763–18775. doi:10.1029/2000ja000455

Crooker, N. U., Eastman, T. E., and Stiles, G. S. (1979). Observations of plasma depletion in the magnetosheath at the dayside magnetopause. *J. Geophys. Res.* 84, 869–874. doi:10.1029/JA084iA03p00869

Dimmock, A. P., Hietala, H., and Zou, Y. (2020). Compiling magnetosheath statistical data sets under specific solar wind conditions: lessons learnt from the dayside kinetic southward IMF GEM challenge. *Earth Space Sci.* 7, e2020EA001095. doi:10.1029/2020EA001095

Dimmock, A. P., and Nykyri, K. (2013). The statistical mapping of magnetosheath plasma properties based on THEMIS measurements in the magnetosheath interplanetary medium reference frame. *J. Geophys. Res. Space Phys.* 118, 4963–4976. doi:10.1002/jgra.50465

Dimmock, A. P., Nykyri, K., and Pulkkinen, T. I. (2014). A statistical study of magnetic field fluctuations in the dayside magnetosheath and their dependence on upstream solar wind conditions. *J. Geophys. Res. Space Phys.* 119, 6231–6248. doi:10.1002/2014JA020009

Dimmock, A. P., Pulkkinen, T. I., Osmane, A., and Nykyri, K. (2016). The dawn-dusk asymmetry of ion density in the dayside magnetosheath and its annual variability measured by THEMIS. *Ann. Geophys.* 34, 511–528. doi:10.5194/angeo-34-511-2016

Dorelli, J. C., Hesse, M., Kuznetsova, M. M., Rastaetter, L., and Raeder, J. (2004). A new look at driven magnetic reconnection at the terrestrial subsolar magnetopause. *J. Geophys. Res. Space Phys.* 109. doi:10.1029/2004ja010458

Fuselier, S. A., Klumpar, D. M., Shelley, E. G., Anderson, B. J., and Coates, A. J. (1991). He^{2+} and H^{+} dynamics in the subsolar magnetosheath and plasma depletion layer. *J. Geophys. Res.* 96, 21095–21104. doi:10.1029/91JA02145

Gershman, D. J., Slavin, J. A., Raines, J. M., Zurbuchen, T. H., Anderson, B. J., Korth, H., et al. (2013). Magnetic flux pileup and plasma depletion in mercury's subsolar magnetosheath. *J. Geophys. Res. Space Phys.* 118, 7181–7199. doi:10.1002/2013ja019244

Hall, D. S., Hapgood, M. A., and Bryant, D. A. (1990). The transition from the magnetosheath to the magnetosphere. *Geophys. Res. Lett.* 17, 2039–2042. doi:10.1029/GL017i011p02039

King, J. H., and Papitashvili, N. E. (2005). Solar wind spatial scales in and comparisons of hourly Wind and ACE plasma and magnetic field data. *J. Geophys. Res. Space Phys.* 110, A02104. doi:10.1029/2004JA010649

Kobel, E., and Fluckiger, E. O. (1994). A model of the steady state magnetic field in the magnetosheath. *J. Geophys. Res.* 99, 23617–23622. doi:10.1029/94JA01778

Longmore, M., Schwartz, S. J., Geach, J., Cooling, B. M. A., Dandouras, I., Lucek, E. A., et al. (2005). Dawn-dusk asymmetries and sub-Alfvénic flow in the high and low latitude magnetosheath. *Ann. Geophys.* 23, 3351–3364. doi:10.5194/angeo-23-3351-2005

Ma, X., Nykyri, K., Dimmock, A., and Chu, C. (2020). Statistical study of solar wind, magnetosheath, and magnetotail plasma and field properties: 12+ years of themis observations and mhd simulations. *J. Geophys. Res. Space Phys.* 125, e2020JA028209. doi:10.1029/2020ja028209

Masters, A., Phan, T. D., Badman, S. V., Hasegawa, H., Fujimoto, M., Russell, C. T., et al. (2014). The plasma depletion layer in saturn's magnetosheath. *J. Geophys. Res. Space Phys.* 119, 121–130. doi:10.1002/2013ja019516

McFadden, J. P., Carlson, C. W., Larson, D., Ludlam, M., Abiad, R., Elliott, B., et al. (2008). The THEMIS ESA plasma instrument and in-flight calibration. *Sci. Stud. Read.* 141, 277–302. doi:10.1007/s11214-008-9440-2

Michotte de Welle, B., Aunai, N., Lavraud, B., Nguyen, G., Génot, V., Ghisalberti, A., et al. (2024). Global environmental constraints on magnetic reconnection at the magnetopause from *in-situ* measurements. *Ess. Open Arch.* doi:10.22541/essoar.170808382.29449499/v1

Michotte de Welle, B., Aunai, N., Nguyen, G., Lavraud, B., Génot, V., Jeandet, A., et al. (2022). Global three-dimensional draping of magnetic field lines in earth's magnetosheath from *in-situ* spacecraft measurements. *J. Geophys. Res. Space Phys.* 127, e2022JA030996. doi:10.1029/2022JA030996

Němeček, Z., Šafránková, J., Zastenker, G. N., Pišoft, P., and Paularena, K. I. (2002). Spatial distribution of the magnetosheath ion flux. *Adv. Space Res.* 30, 2751–2756. doi:10.1016/S0273-1177(02)80402-1

Nguyen, G., Aunai, N., Michotte de Welle, B., Jeandet, A., Lavraud, B., and Fontaine, D. (2022). Massive multi-mission statistical study and analytical modeling of the earth's magnetopause: 1. A gradient boosting based automatic detection of near-earth regions. *J. Geophys. Res. Space Phys.* 127, e29773. doi:10.1029/2021JA029773

Øieroset, M., Mitchell, D. L., Phan, T. D., Lin, R. P., Crider, D. H., and Acuña, M. H. (2004). The magnetic field pile-up and density depletion in the martian magnetosheath: a comparison with the plasma depletion layer upstream of the earth's magnetopause. *Space Sci. Rev.* 111, 185–202. doi:10.1023/b:spac.0000032715.69695.9c

Paschmann, G., Baumjohann, W., Sckopke, N., Phan, T. D., and Luehr, H. (1993). Structure of the dayside magnetopause for low magnetic shear. *J. Geophys. Res.* 98, 13409–13422. doi:10.1029/93JA00646

Paschmann, G., Sckopke, N., Haerendel, G., Papamastorakis, J., Bame, S. J., Asbridge, J. R., et al. (1978). ISEE plasma observations near the subsolar magnetopause article published in the special issues: advances in magnetospheric physics with GEOS- 1 and ISEE - 1 and 2. *Space Sci. Rev.* 22, 717–737. doi:10.1007/BF00212620

Paularena, K. I., Richardson, J. D., Kolpak, M. A., Jackson, C. R., and Siscoe, G. L. (2001). A dawn-dusk density asymmetry in Earth's magnetosheath. *Earth's magnetosheath* 106, 25377–25394. doi:10.1029/2000JA000177

Phan, T. D., Paschmann, G., Baumjohann, W., Sckopke, N., and Luehr, H. (1994). The magnetosheath region adjacent to the dayside magnetopause: AMPTE/IRM observations. *J. Geophys. Res.* 99, 121–141. doi:10.1029/93JA02444

Pollock, C., Moore, T., Jacques, A., Burch, J., Gliese, U., Saito, Y., et al. (2016). Fast plasma investigation for magnetospheric multiscale. *Sci. Stud. Read.* 199, 331–406. doi:10.1007/s11214-016-0245-4

Pudovkin, M. I., Besser, B. P., Zaitseva, S. A., Lebedeva, V. V., and Meister, C. V. (2001). Magnetic barrier in case of a southward interplanetary magnetic field. *J. Atmos. Solar-Terrestrial Phys.* 63, 1075–1083. doi:10.1016/S1364-6826(01)00023-2

Rème, H., Aoustin, C., Bosqued, J. M., Dand ouras, I., Lavraud, B., Sauvaud, J. A., et al. (2001). First multispacecraft ion measurements in and near the Earth's magnetosphere with the identical Cluster ion spectrometry (CIS) experiment. *Ann. Geophys.* 19, 1303–1354. doi:10.5194/angeo-19-1303-2001

Rème, H., Dandouras, I., Aoustin, C., Bosqued, J. M., Sauvaud, J. A., Vallat, C., et al. (2005). The HIA instrument on board the Tan Ce 1 Double Star near-equatorial spacecraft and its first results. *Ann. Geophys.* 23, 2757–2774. doi:10.5194/angeo-23-2757-2005

Romashets, E. P., and Vandas, M. (2019). Analytic modeling of magnetic field in the magnetosheath and outer magnetosphere. *J. Geophys. Res. Space Phys.* 124, 2697–2710. doi:10.1029/2018JA026006

Russell, C. T., Anderson, B. J., Baumjohann, W., Bromund, K. R., Dearborn, D., Fischer, D., et al. (2016). The magnetospheric multiscale magnetometers. *Sci. Stud. Read.* 199, 189–256. doi:10.1007/s11214-014-0057-3

Šafránková, J., Přech, L., Němeček, Z., and Sauvaud, J. A. (2002). Density profile in the magnetosheath adjacent to the magnetopause. *Adv. Space Res.* 30, 1693–1703. doi:10.1016/S0273-1177(02)00438-6

Sibeck, D. G., Lepping, R. P., and Lazarus, A. J. (1990). Magnetic field line draping in the plasma depletion layer. *J. Geophys. Res. Space Phys.* 95, 2433–2440. doi:10.1029/ja095ia03p02433

Song, P., Russell, C. T., Gosling, J. T., Thomsen, M., and Elphic, R. C. (1990). Observations of the density profile in the magnetosheath near the stagnation streamline. *Geophys. Res. Lett.* 17, 2035–2038. doi:10.1029/GL017i011p02035

Spreiter, J. R., Summers, A. L., and Alksne, A. Y. (1966). Hydromagnetic flow around the magnetosphere. *Planet. Space Sci.* 14, 223–253. doi:10.1016/0032-0633(66)90124-3

Trattner, K. J., Petrinec, S. M., and Fuselier, S. A. (2021). The location of magnetic reconnection at earth's magnetopause. *Earth's Magnetopause* 217, 41. doi:10.1007/s11214-021-00817-8

Walsh, B. M., Sibeck, D. G., Wang, Y., and Fairfield, D. H. (2012). Dawn-dusk asymmetries in the Earth's magnetosheath. *J. Geophys. Res. Space Phys.* 117, A12211. doi:10.1029/2012JA018240

Walters, G. K. (1964). Effect of oblique interplanetary magnetic field on shape and behavior of the magnetosphere. *J. Geophys. Res.* 69, 1769–1783. doi:10.1029/JZ069i009p01769

Wang, Y., Raeder, J., and Russell, C. (2004a). Plasma depletion layer: its dependence on solar wind conditions and the Earth dipole tilt. *Ann. Geophys.* 22, 4273–4290. doi:10.5194/angeo-22-4273-2004

Wang, Y., Raeder, J., and Russell, C. (2004b). Plasma depletion layer: magnetosheath flow structure and forces. *Ann. Geophys.* 22, 1001–1017. doi:10.5194/angeo-22-1001-2004

Wang, Y. L., Raeder, J., Russell, C. T., Phan, T. D., and Manapat, M. (2003). Plasma depletion layer: event studies with a global model. *J. Geophys. Res. Space Phys.* 108, 1010. doi:10.1029/2002JA009281

Wu, C. C. (1992). Mhd flow past an obstacle: large-scale flow in the magnetosheath. *Geophys. Res. Lett.* 19, 87–90. doi:10.1029/91gl03007

Zhang, H., Fu, S., Pu, Z., Lu, J., Zhong, J., Zhu, C., et al. (2019). Statistics on the magnetosheath properties related to magnetopause magnetic reconnection. *Astrophys. J.* 880, 122. doi:10.3847/1538-4357/ab290e

Zwan, B. J., and Wolf, R. A. (1976). Depletion of solar wind plasma near a planetary boundary. *J. Geophys. Res.* 81, 1636–1648. doi:10.1029/JA081i010p01636